Local cyclical compression modulates macrophage function in situ and alleviates immobilization-induced muscle atrophy

Journal Article

Author(s):
Saitou, Kumiko; Tokunaga, Masakuni; Yoshino, Daisuke; Sakitani, Naoyoshi; Maekawa, Takahiro; Ryu, Youngjae; Nagao, Motoshi; Nakamoto, Hideki; Saito, Taku; Kawanishi, Noriaki; Suzuki, Katsuhiko; Ogata, Toru; Makuuchi, Michiru; Takashima, Atsushi; Sawada, Keisuke; Kawamura, Shunsuke; Nakazato, Koichi; Kouzaki, Karina; Harada, Ichiro; Ichihara, Yoshinori; Sawada, Yasuhiro

Publication date:
2018-10

Permanent link:
https://doi.org/10.3929/ethz-b-000302365

Originally published in:
Clinical Science 132(19), https://doi.org/10.1042/CS20180432

Clinical Science (2018) **132** 2147–2161
https://doi.org/10.1042/CS20180432

Research Article

Local cyclical compression modulates macrophage function *in situ* and alleviates immobilization-induced muscle atrophy

Kumiko Saitou[1,2], Masakuni Tokunaga[1], Daisuke Yoshino[3], Naoyoshi Sakitani[1], Takahiro Maekawa[1], Youngjae Ryu[1], Motoshi Nagao[1], Hideki Nakamoto[4], Taku Saito[4], Noriaki Kawanishi[5], Katsuhiko Suzuki[6], Toru Ogata[1], Michiru Makuuchi[7], Atsushi Takashima[8], Keisuke Sawada[9], Shunsuke Kawamura[10], Koichi Nakazato[11], Karina Kouzaki[11], Ichiro Harada[12], Yoshinori Ichihara[1,13] and Yasuhiro Sawada[1,14]

[1]Department of Rehabilitation for Motor Functions, National Rehabilitation Center for Persons with Disabilities, 4-1 Namiki, Tokorozawa, Saitama 359-8555, Japan; [2]Graduate School of Sport Sciences, Waseda University, 2-579-15 Mikajima, Tokorozawa, Saitama 359-1192, Japan; [3]Frontier Research Institute for Interdisciplinary Sciences, Tohoku University, 6-3 Aramaki-aza-Aoba, Aoba, Sendai, Miyagi 980-8578, Japan; [4]Department of Orthopaedic Surgery, Graduate School of Medicine, The University of Tokyo, 7-3-1 Hongo, Bunkyo, Tokyo 113-0033, Japan; [5]Faculty of Advanced Engineering, Chiba Institute of Technology, 2-1-1 Shibazono, Narashino, Chiba 275-0023, Japan; [6]Faculty of Sport Sciences, Waseda University, 2-579-15 Mikajima, Tokorozawa, Saitama 359-1192, Japan; [7]Section of Neuropsychology, National Rehabilitation Center for Persons with Disabilities, 4-1 Namiki, Tokorozawa, Saitama 359-8555, Japan; [8]Department of Assistive Technology, National Rehabilitation Center for Persons with Disabilities, 4-1 Namiki, Tokorozawa, Saitama 359-8555, Japan; [9]Department of Pathology, Cell Pathology Division, The Children's Hospital of Philadelphia, Philaldelphia, PA 19104, U.S.A.; [10]Department of Biosystems Science and Engineering, ETH Zürich, Mattenstrasse 26, Basel 4058, Switzerland; [11]Graduate School of Health and Sport Sciences, Nippon Sport Science University, 7-1-1 Fukasawa, Setagaya, Tokyo 158-8508, Japan; [12]Nadogaya Institute, Nadogaya Hospital, 687-4 Nadogaya, Kashiwa, Chiba 277-0032, Japan; [13]Division of Pharmacology, Faculty of Medicine, Tottori University, 86 Nishi-cho, Yonago, Tottori 683-8503, Japan; [14]Department of Clinical Research, National Rehabilitation Center for Persons with Disabilities, 4-1 Namiki, Tokorozawa, Saitama 359-8555, Japan

Correspondence: Yasuhiro Sawada (ys454-ind@umin.ac.jp)

Physical inactivity gives rise to numerous diseases and organismal dysfunctions, particularly those related to aging. Musculoskeletal disorders including muscle atrophy, which can result from a sedentary lifestyle, aggravate locomotive malfunction and evoke a vicious circle leading to severe functional disruptions of vital organs such as the brain and cardiovascular system. Although the significance of physical activity is evident, molecular mechanisms behind its beneficial effects are poorly understood. Here, we show that massage-like mechanical interventions modulate immobilization-induced pro-inflammatory responses of macrophages *in situ* and alleviate muscle atrophy. Local cyclical compression (LCC) on mouse calves, which generates intramuscular pressure waves with amplitude of 50 mmHg, partially restores the myofiber thickness and contracting forces of calf muscles that are decreased by hindlimb immobilization. LCC tempers the increase in the number of cells expressing pro-inflammatory proteins, tumor necrosis factor-α and monocyte chemoattractant protein-1 (MCP-1), including macrophages *in situ*. The reversing effect of LCC on immobilization-induced thinning of myofibers is almost completely nullified when macrophages recruited from circulating blood are depleted by administration of clodronate liposomes. Furthermore, application of pulsatile fluid shear stress, but not hydrostatic pressure, reduces the expression of MCP-1 in macrophages *in vitro*. Together with the LCC-induced movement of intramuscular interstitial fluid detected by μCT analysis, these results suggest that mechanical modulation of macrophage function is involved in physical inactivity-induced muscle atrophy and inflammation. Our findings uncover the implication of mechanosensory function of macrophages in disuse muscle atrophy, thereby opening a new path to develop a novel therapeutic strategy utilizing mechanical interventions.

Received: 14 July 2018
Revised: 10 September 2018
Accepted: 11 September 2018

Accepted Manuscript Online: 12 September 2018
Version of Record published: 12 October 2018

Clinical Science (2018) **132** 2147–2161
https://doi.org/10.1042/CS20180432

Introduction

Physical inactivity, the fourth leading risk factor for death worldwide, kills more than 5 million people every year [1]. It arises from a variety of health problems including aging, injury, and neuromuscular diseases and can lead to numerous organismal disorders such as muscle atrophy [2]. Inflammation, which involves enhanced expression or production of pro-inflammatory cytokines and chemokines, has been implicated in the pathology of disuse muscle atrophy [3,4]. In addition to the chronic nature of inactivity-related inflammation [5], a vicious circle formed by physical inactivity and muscle weakness exacerbates loss of muscle mass, resulting in irreversible deterioration of general bodily functions.

Physical exercise has anti-inflammatory effects [6,7]. However, the molecular mechanisms underlying the benefits of exercise to organismal homeostasis are poorly understood, especially with regard to its suppression of local inflammation. This problem may partially account for the small population partaking in habitual exercise [8,9] and the lack of guidelines for physical exercise as a therapeutic/preventative intervention in lifestyle-related diseases and disorders including muscle atrophy.

Massage is generally appreciated as a pain- or inflammation-relieving procedure, being recognized to be beneficial for both pain relief and improvement of physical performance for both competitive athletes and non-athletes alike [10,11]. In fact, massage reportedly suppresses local inflammation [12] and prompts recovery from postexercise muscle damage [13,14]. Although little is known about the molecular mechanisms behind the beneficial effects of massage, there is a common feature between physical exercise and massage. They both generate local mechanical forces on organs, tissues, and cells. Taken together with the anti-inflammatory effects of both exercise and massage [14-16], we hypothesized that mechanical forces generated by massage or massage-like interventions might modulate local inflammatory processes underlying disuse muscle atrophy.

Macrophages play important roles in the regulation of various immune responses and inflammatory processes [17,18]. In the context of organismal homeostasis, macrophages are critically involved in many age-related disorders including diabetes mellitus [19], atherosclerosis [20], Alzheimer's disease [21], and cancer [22]. To test our hypothesis mentioned above, we examined whether massage-like interventions affected local inflammatory processes involving cellular responses to mechanical forces in skeletal muscle tissues, with particular reference to macrophage function and behavior.

Materials and methods

Animals

All animal experiments were approved by the Institutional Animal Care and Use Committee of National Rehabilitation Center for Persons with Disabilities. C57BL/6J mice purchased from Charles River Laboratories (Yokohama, Japan) were housed with free access to water and standard rodent chow under a 12-h light/dark cycle at $22 \pm 2^{\circ}$C and constant humidity ($55 \pm 10\%$). Male mice were subjected to experiments at the age of 11–12 weeks after an acclimation for at least 7 days, with an exception of peritoneal macrophage isolation in which 8- to 10-week-old female mice were used.

Antibodies and chemicals

Rat monoclonal anti-laminin-2 antibody (Cat# L0663) was purchased from Sigma-Aldrich (St. Louis, MO). Rat monoclonal anti-F4/80 antibody (Cat# ab6640), rabbit polyclonal anti-MCP-1 antibody (Cat# ab25124), and rabbit polyclonal anti-TNF-α antibody (Cat# ab66579) were purchased from Abcam (Cambridge, U.K.). Goat anti-rabbit Alexa Fluor 488 (Cat# A11034) and goat anti-rat Alexa Fluor 568 (Cat# A11077) were purchased from Invitrogen (Carlsbad, CA). Clodronate liposome (Clophosome-A) and its control liposome were purchased from FormuMax Scientific (Sunnyvale, CA). Sodium pentobarbital was purchased from Kyoritu Seiyaku (Tokyo, Japan). The other chemicals were purchased from Sigma-Aldrich unless noted otherwise.

Immobilization of mouse bilateral hindlimbs

Bilateral hindlimbs of mice were immobilized as described previously [23]. Surgical tape (3M Japan, Tokyo, Japan) and aluminum wire (Eko Metal, Niigata, Japan) were applied to mice under hypnosis with sodium pentobarbital (50 mg/kg i.p.) so that the motions of their bilateral hindlimbs were restricted with their hip joints abducted, knee joints extended, and ankle joints plantar-flexed for defined periods (Figure 1A).

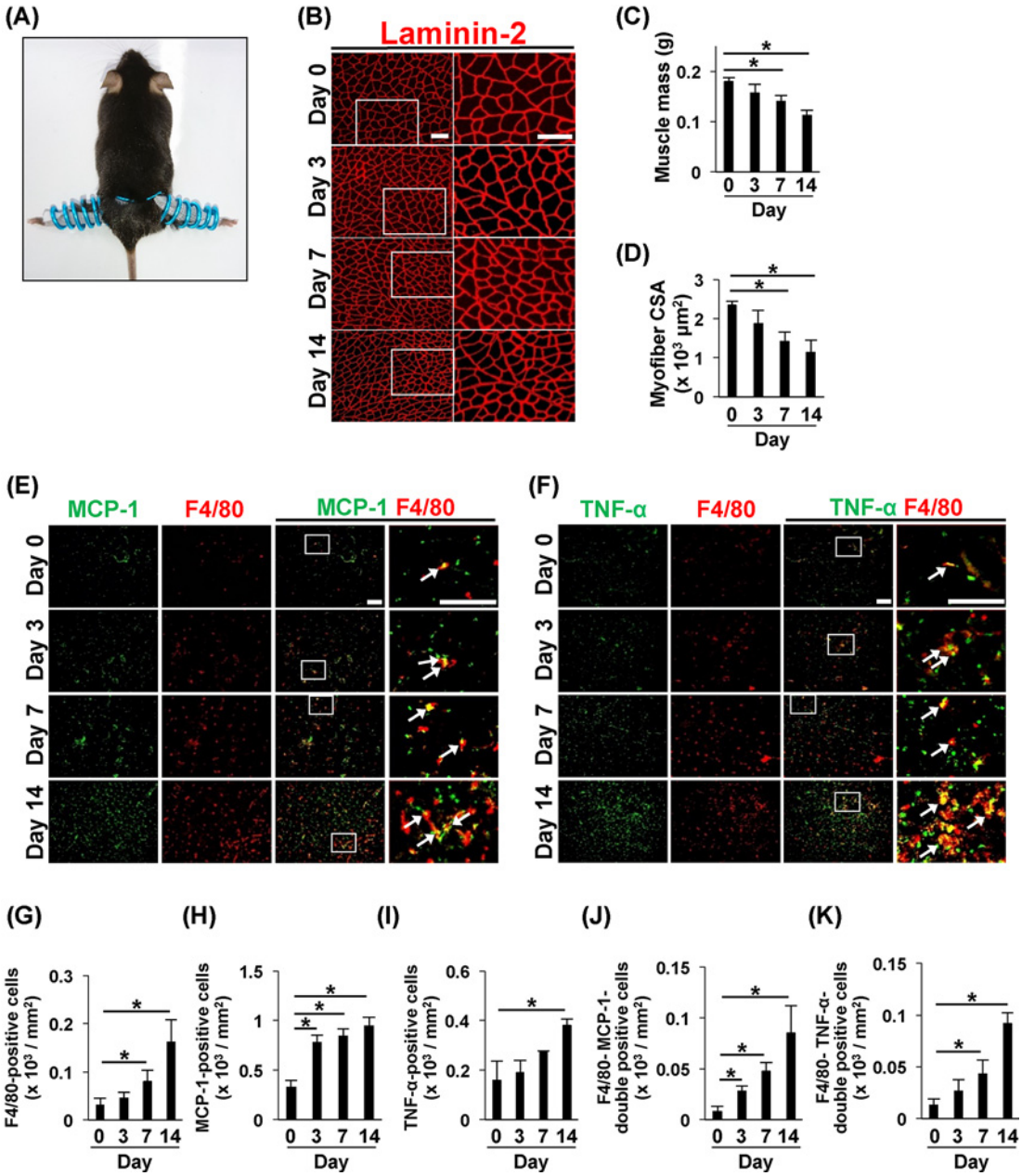

Figure 1. Mouse hindlimb immobilization, which atrophies calf muscles, induces local inflammatory response

(**A**) Bilateral hindlimb immobilization. Deformable metal wire was adjusted to immobilize bilateral hindlimbs of mice. (**B**) Cross-sectional micrographic images of anti-laminin-2 immunofluorescence staining of gastrocnemius muscles. High magnification images (right) refer to the areas indicated by rectangles in low magnification images (left); scale bars, 100 μm. (**C** and **D**) Immobilization-induced muscle atrophy. Triceps surae muscle mass (C) and CSA of gastrocnemius myofibers (D) decreased with the period of hindlimb immobilization. To quantify CSA, 100 myofibers were randomly chosen. Data are presented as means ± S.D. *$P<0.05$, one-way ANOVA with post hoc Bonferroni test ($n = 3$ mice for each group). (**E** and **F**) Micrographic images of anti-MCP-1 (green in E) and anti-TNF-α (green in F) and anti-F4/80 (red) immunostaining. For merged presentation (green and red), low and high magnification images are laid as in (B). Arrows point to double positive cells for F4/80 and MCP-1 (E) or TNF-α (F); scale bars, 100 μm. (**G–K**) Quantification of anti-MCP-1, anti-TNF-α, and anti-F4/80 immunostaining. Data are presented as means ± S.D. *$P<0.05$, one-way ANOVA with post hoc Bonferroni test ($n = 3$ mice for each group).

Clinical Science (2018) **132** 2147–2161
https://doi.org/10.1042/CS20180432

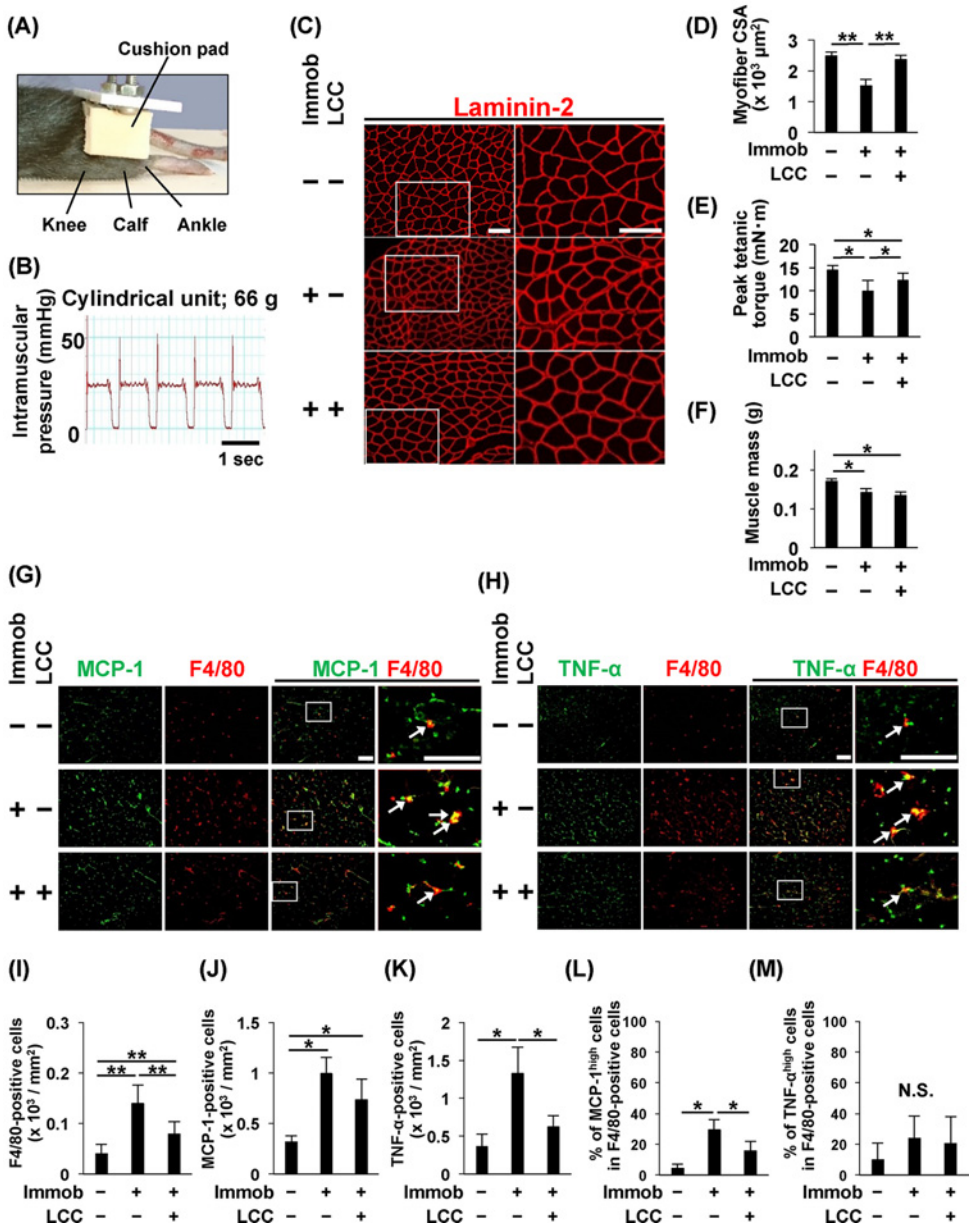

Figure 2. LCC modulates macrophage function and attenuates immobilization-induced muscle atrophy and inflammatory response

(**A**) Experimental set-up for LCC. (**B**) Intramuscular pressure waves during LCC; scale bar, 1 s. LCC application on mouse calves using a 66-g cylindrical unit produced intramuscular pressure waves with amplitude of 50 mmHg. (**C**) Cross-sectional micrographic images of anti-laminin-2 immunofluorescence staining of gastrocnemius muscles. High and low magnification images are presented as in Figure 1B; scale bars, 100 μm. (**D–F**) Alleviation of immobilization-induced muscle atrophy by LCC application. CSA of gastrocnemius myofibers (D) and triceps surae muscle mass (F) were analyzed as in Figure 1D,C, respectively. Data are presented as means ± S.D. *$P<0.05$; **$P<0.01$, one-way ANOVA with post hoc Bonferroni test ($n = 6$ mice for each group). (E) Decrease in contracting force of triceps surae muscles after immobilization and its partial restoration by LCC. Data are presented as means ± S.D. *$P<0.05$, paired Student's t test ($n = 4$ mice for control; $n = 5$ mice for immobilization group). (**G** and **H**) Micrographic images of anti-MCP-1 (green in G), anti-TNF-α (green in H) and anti-F4/80 (red) immunofluorescence staining of gastrocnemius muscles of unimmobilized (top) and immobilized hindlimbs without (middle) and with (bottom) LCC application are presented as in Figure 1E,F; scale bars, 100 μm. (**I–M**) Quantification of anti-MCP-1, anti-TNF-α, and anti-F4/80 immunostaining. The anti-MCP-1 and anti-TNF-α immunosignals with the intensities higher than 50% of the highest ones in the respective staining were defined as MCP-1^{high} (L) and TNF-α^{high} (M), respectively. Data are presented as means ± S.D.; N.S., not significant, *$P<0.05$; **$P<0.01$, one-way ANOVA with post hoc Bonferroni test ($n = 6$ mice for each group).

Local cyclical compression on mouse calves

Hindlimb-immobilized mice were hypnotized with sodium pentobarbital, temporarily disengaged from wiring (see Supplementary Figure S1A), and laid at a prone position with their knee joints extended and ankle joints plantar-flexed so that their calves faced upward. Local cyclical compression (LCC) was applied by vertically moving a cylindrical weight unit covered with a cushion pad (Figure 2A). After LCC application for 30 min, mouse hindlimbs were re-coiled to continue immobilization. Among the several different LCC magnitudes we tested by changing the weight of the cylindrical unit (Figure 2B and Supplementary Figure S2A), the one that produced 50 mmHg intramuscular (gastrocnemius) pressure waves (Figure 2B) appeared to be optimal in terms of alleviation of immobilization-induced muscle atrophy and local macrophage accumulation (Supplementary Figure S2B). We also confirmed that LCC of this mode/magnitude did not generate apparent muscle damage at a microscopic level (Supplementary Figure S2C). We therefore employed this LCC set-up for further studies. LCC side (right or left) was chosen randomly.

Selective depletion of monocytes/macrophages recruited from circulating blood

To deplete phagocytic cells recruited from circulating blood, mice were administered with clodronate liposome according to the manufacturer's instructions, i.e., 200 μl i.p. for single administration [24], and the first 150 μl i.p. followed by 100 μl i.p. every 3 days for repeated administration [25]. Clodronate liposome (or control liposome) injection during the period of hindlimb immobilization was carried out just before re-wiring mouse hindlimbs, which had been temporarily disengaged from immobilization for the purpose of daily LCC application (see Supplementary Figure S1B).

Morphological analysis of blood cells

Circulating blood was collected in a tripotassium EDTA-containing tube (Terumo, Tokyo, Japan) from the inferior vena cava of mice anesthetized with intraperitoneal injection of a mixture of three anesthetic agents (medetomidine 0.75 mg/kg, midazolam 4.0 mg/kg, butorphanol 5.0 mg/kg). A thin smear of blood on a slide was dried, fixed in methanol, and subjected to Wright–Giemsa staining [26] using Wright's (Muto Pure Chemicals, Tokyo, Japan) and Giemsa's (Nacalai Tesque, Kyoto, Japan) solutions diluted with pH 6.4 phosphate buffer (LSI Medience, Tokyo, Japan). Differential counting was conducted for 100 white blood cells in each sample.

Immunohistochemical analysis of calf muscle tissues

Immediately after killing mice by cervical dislocation, triceps surae muscles were dissected, quickly frozen in an optimal cutting temperature compound solution (Sakura Finetek, Torrance, CA), and subjected to cryostat (CM3050 S, Leica Biosystems, Eisfeld, Germany) sectioning with 20 μm thickness. Specimens mounted on glass slides were incubated in blocking buffer (Protein Block Serum-Free, Dako, Carpinteria, CA) for 30 min at room temperature, and then with primary antibodies overnight at room temperature followed by Alexa Fluor 488- or 568-conjugated secondary antibodies for 1 h at room temperature. Both primary and secondary antibodies were diluted in a Tris-HCl buffer (REAL™ Antibody Diluent, Dako, Carpinteria, CA). Nuclei were counterstained with DAPI (Thermo Fisher Scientific, Waltham, MA). After mounting with an antifade reagent (Prolong Gold, Thermo Fisher Scientific), specimens were viewed using a fluorescence microscope (BZ-9000, Keyence, Osaka, Japan).

Histomorphometrical analysis of muscle tissues

Mouse calf muscles were histomorphometrically analyzed at their 1/3 proximal levels, where their bellies appeared thickest. The cross-sectional area (CSA) of each myofiber was determined by tracing the 'internal' margin of the basement membrane visualized with anti-laminin-2 immunostaining (cyan dot line in Supplementary Figure S2D). Interstitial space surrounding individual myofiber was defined by tracing the 'external' margin of the basement membrane (yellow dot line in Supplementary Figure S2D). Microscopic images were analyzed using ImageJ software (NIH, Bethesda, MD). Cells positively stained with F4/80, a marker for macrophage [27], were defined as macrophages.

Isolation of peritoneal macrophages

Mouse peritoneal macrophages were isolated as described previously [28,29]. Briefly, 3 days after 8- to 10-week-old female C57BL/6J mice were administered with 5 ml of Brewer thioglycollate medium (3% w/v in distilled water, i.p.), their peritoneal cavities were filled with cold 5 ml of phosphate-buffered saline (PBS), and then kneaded gently for 3 min. Injected PBS was collected using a 21-gauge needle, and centrifuged at 100 *g* for 5 min to sediment a cell pellet.

Clinical Science (2018) **132** 2147–2161
https://doi.org/10.1042/CS20180432

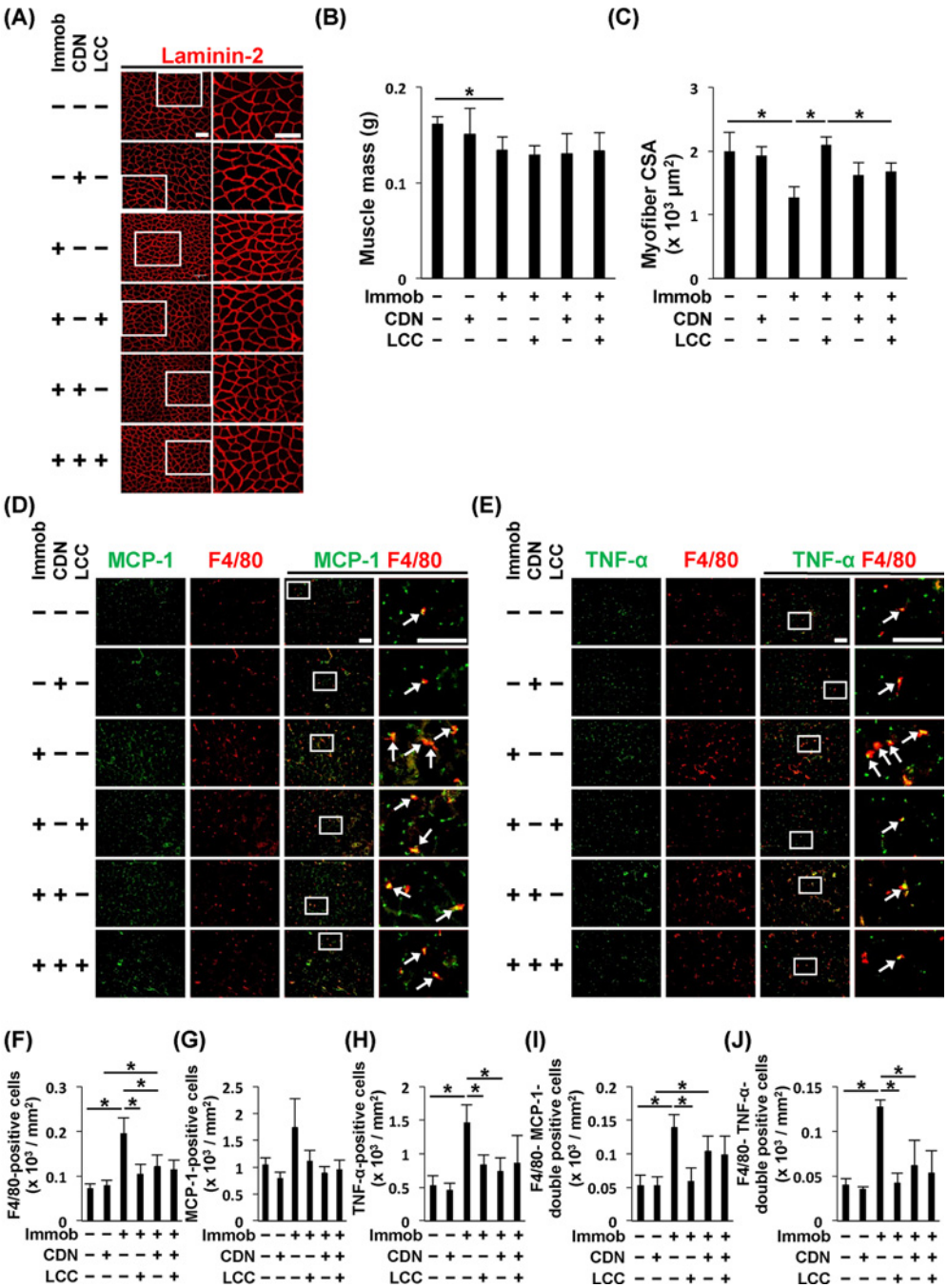

Figure 3. Depletion of macrophages recruited from blood alleviates immobilization-induced muscle atrophy and inflammatory responses, eliminating the effect of LCC

(**A**) Micrographic images of anti-laminin-2 immunofluorescence staining of gastrocnemius muscles. High and low magnification images are presented as in Figure 1B; scale bars, 100 μm. (**B** and **C**) Clodronate liposome administration alleviated hindlimb immobilization-induced muscle atrophy and eliminates the increase in myofiber CSA by LCC. Triceps surae muscle mass (B) and CSA of gastrocnemius myofibers (C) were quantified as in Figure 1C,D. Data are presented as means ± S.D. *P<0.05, unpaired Student's t test (n = 5 mice for each group of control liposome administration; n = 6 mice for each group of clodronate liposome administration). (**D** and **E**) Micrographic images of anti-MCP-1 (green in D), anti-TNF-α (green in E), and anti-F4/80 (red) immunofluorescence staining. For merged presentation (green and red), low and high magnification images are presented as in Figure 1E,F; scale bars, 100 μm. (**F–J**) Quantification of anti-MCP-1, anti-TNF-α, and anti-F4/80 immunostaining. Data are presented as means ± S.D. *P<0.05, one-way ANOVA with post hoc Bonferroni test (n = 5 mice for each group of control liposome administration; n = 6 mice for each group of clodronate liposome administration).

Cells were resuspended in RPMI-1640 (Thermo Fisher Scientific) containing 10% fetal bovine serum (GE Healthcare, Uppsala, Sweden) and seeded on a plastic dish. After 24 h, non-adherent cells were removed by two-times wash with PBS. Consistent with previous reports [30], we confirmed that 70–80% of remaining adherent cells were positive for F4/80.

Application of fluid shear stress or hydrostatic pressure to cultured macrophages

Mouse peritoneal macrophages pre-treated with LPS (100 ng/ml) for 24 h were exposed to pulsatile fluid shear stress (FSS) with an average magnitude of 0.5 Pa at a frequency of 0.5 Hz for 30 min using a custom-made flow system as described previously [31] with slight modifications. A flow-chamber, which was composed of a cell culture dish, a polycarbonate I/O unit and a silicone gasket, generated a 22.5-mm-wide 35-mm-long 0.5-mm-high flow channel (Supplementary Figure S3A). Macrophages were seeded at a density of 4×10^5 cells/8.0 cm^2. The system was adjusted to generate pressure waves with amplitude of 50 mmHg (zero to peak) and placed in a CO_2 incubator to maintain pH and temperature of culture medium.

As a control for FSS, macrophages seeded at a density of 3×10^5 cells/6.6 cm^2 were exposed to pulsatile hydrostatic pressure (HP) with amplitude of 50 mmHg (zero to peak) at a frequency of 0.5 Hz for 30 min using a custom-made pressure system described previously [32] with slight modifications. The system consists of a cell culture dish, a polycarbonate pressure chamber, a silicone gasket, an O-ring, a quartz glass, two holding jigs, a thermostatic chamber, and a syringe pump (Supplementary Figure S3B). The entire system was completely airtight, enabling precise and strict pressure control with the syringe pump. In both FSS and HP experiments, cell adhesion and morphology were observed using a light microscope (DM IRE2, Leica Microsystems, Wetzlar, Germany).

RNA extraction and real-time quantitative PCR

Six hours after the termination of FSS or HP application, peritoneal macrophages were subjected to total RNA extraction using guanidine thiocyanate (ISOGEN, Nippon Gene, Tokyo, Japan) followed by reverse transcription using both oligo(dT) and random hexamers as primers (PrimeScript RT Reagent Kit, Takara Bio, Shiga, Japan) to generate cDNA. We subjected cDNA to real-time quantitative PCR reactions in duplicates using a thermal cycler (ABI Prism 7500, Applied Biosystems, Foster City, CA). Data were analyzed using sequence detection system software (7500 System SDS, Applied Biosystems, Foster City, CA) and relative mRNA abundance was normalized to GAPDH. $\Delta\Delta C_t$ method was applied for comparison of expression levels. The sequences of the primers used in study were as follows. *Gapdh*; 5′-TGCACCACCAACTGCTTAGC-3′ (forward) and 5′- GGATGCAGGGATGATGTTCT-3′ (reverse), *Mcp-1*; 5′-GCTCTCTCTTCCTCCACCAC-3′ (forward) and 5′-GCTTCTTTGGGACACCTGCT-3′ (reverse), *Tnf-α*; 5′-CCTGTAGCCCACGTCGTAG-3′ (forward) and 5′-GGGAGTAGACAAGGTACAACCC-3′ (reverse), *Tgf-β1*; 5′-AAGTTGGCATGGTAGCCCTT-3′ (forward) and 5′-GCCCTGGATACCAACTATTGC-3′ (reverse), *Cd206*; 5′-TTCAGCTATTGGACGCGAGG-3′ (forward) and 5′-GAATCTGACACCCAGCGGAA-3′ (reverse).

Measurement of intramuscular pressure of mouse gastrocnemius muscles

Under anesthesia with intraperitoneal injection of a mixture of three anesthetic agents, 11- to 12-week-old male mice were subjected to intramuscular pressure measurement. Through a posterior skin incision on the calf, a 20-gauge indwelling needle was inserted to the gastrocnemius muscle at an obtuse angle. Using its plastic sheath as a guide, a sensor of blood pressure telemeter (Millar, Houston, TX) was placed in the mid-belly of the muscle. After suturing the skin, intramuscular pressure was monitored using LabChart8 (ADInstruments Japan, Nagoya, Japan).

μCT imaging of the dynamics of intramuscular interstitial fluid

Eleven- to twelve-week-old male mice anesthetized with a mixture of three anesthetic agents (i.p) were subjected to microinjection of an iodine-based contrast medium (Isovist® inj. 300, Bayer, Berlin, Germany), followed by μCT imaging. After exposing fascia through 2-mm posterior skin incision on the calf, a 31-gauge needle was inserted to the depth of 2 mm to locate its bevel tip in the mid-belly of gastrocnemius muscle. Using a microsyringe (Microliter Syringe, Hamilton, NV) and a stereotaxic injector (Legato130, Muromachi, Tokyo, Japan), 3 μl of contrast medium was infused with the rate fixed at 0.6 μl/min. After completing the infusion, we held the microsyringe for 5 min to avoid reflux, pulled out the needle carefully, closed the skin with a tissue adhesive (3M Vetbond, St. Paul, MN), and set the mice in a CT scanner (inspeXio SMX-100CT, Shimadzu, Kyoto, Japan). Mice were subjected to two serial

Clinical Science (2018) **132** 2147–2161
https://doi.org/10.1042/CS20180432

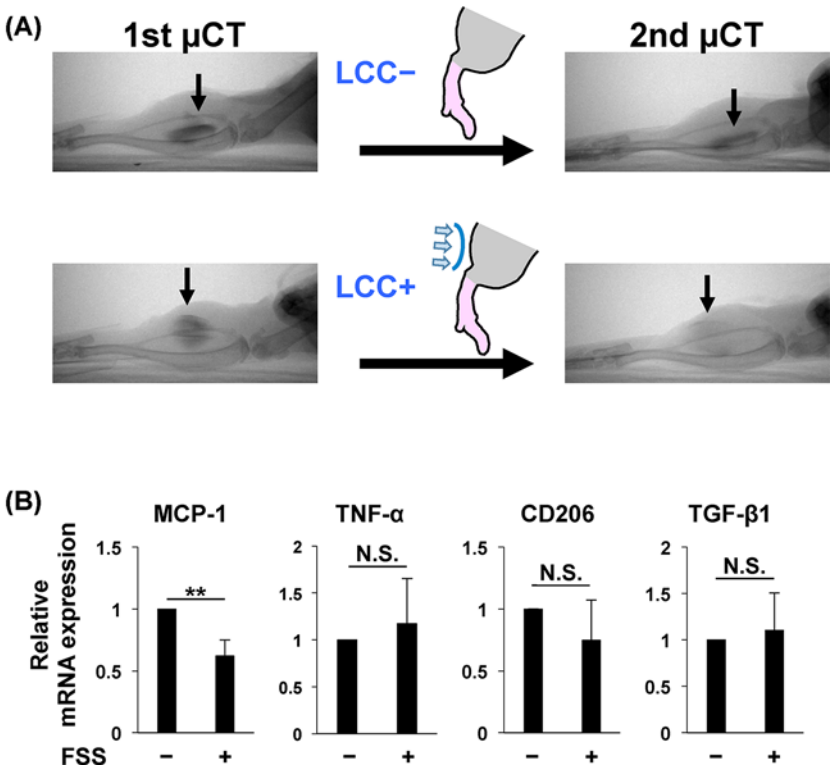

Figure 4. Analysis of intramuscular interstitial fluid dynamics during LCC *in vivo* and responses of macrophages to mechanical stresses *in vitro*

(**A**) Representative X-ray radiographs imaging contrast medium (Isovist) injected into gastrocnemius muscle bellies of mice, either exposed or left unexposed to LCC on their calves for 5 s. LCC was applied between the first and second imaging (see Supplementary Figure S1C). Arrows point to Isovist clusters. (**B**) FSS decreased mRNA expression of MCP-1 in cultured macrophages. LPS-pretreated peritoneal macrophages were either exposed or left unexposed to pulsatile FSS (frequency; 0.5 Hz, average magnitude 0.5 Pa, zero-to-peak mode) for 30 min. Six hours after the termination of FSS application, macrophages were subjected to total RNA extraction followed by quantitative PCR analysis. mRNA expression levels were normalized against GAPDH, and scaled with the control sample (FSS-) set at 1 in each experiment. Data are presented as means ± S.D. N.S., not significant, $^{**}P<0.01$, paired Student's t test ($n=5$).

hindlimb μCT scans between which LCC was either applied or left unapplied (kept sedentary) for 5 s (see Supplementary Figure S1C). μCT images were obtained with following parameters: voxel size 50 μm, 60 KeV, 58 μA, field of view 25.6 mm, matrix size 512 × 512 (Supplementary Figure S4A). 3D reconstructed objects were visualized and analyzed on software for 3D histomorphometry (TRI/3D-BON-FCS64, RATOC System, Tokyo, Japan). The contrast medium cluster in muscle belly was defined as voxels with ≥1.2 times signal intensity as compared with that of muscle parenchyma (Supplementary Figure S4B).

Measurement of contracting forces of mouse triceps surae muscles

Triceps surae muscle contracting forces were measured by the electrical stimulation method that we reported previously [33]. Under anesthesia with a mixture of three anesthetic agents (i.p.), 11- to 12-week-old male mice were placed in a prone position with their hemilateral feet on a footplate fixed on a rotatory disc (knee joint extended and ankle joint at 90°) to quantify the torques. A surface electrode connected to an electric stimulator and an isolator (SS-104J; Nihon Kohden, Tokyo, Japan) was attached on their pelage-cleared calves to induce their triceps surae muscles to contract isometrically. We defined the muscle contracting forces as the torques generated at the maximal tetanic contractions (peak tetanic torques) elicited by the electrical stimulation with rectangular pulses (duration, 4 ms; frequency, 100 Hz). The stimulation intensity for the maximal contraction, which was determined by varying single stimuli in each sample, ranged from 15 to 20 V.

Simulative calculation of the magnitude of interstitial fluid flow-derived shear stress during LCC

The spreading of contrast medium was dominantly observed along the direction of myofibers (Figure 4A and Supplementary Figure S4B). We therefore compared the longitudinal distances of contrast medium spreading between two serial μCT images of mouse hindlimbs with and without LCC application, and evaluated LCC-induced displacement of contrast medium (Supplementary Figure S4C). Based on these measurements, we calculated the velocity of interstitial fluid movement induced by LCC.

We assumed that interstitial fluid flow in the muscle tissue follows the Henry Darcy's law, which defines the flux density of penetrating fluid per unit time. The velocity of interstitial fluid flow (u) is assumed to approach the superficial velocity (u_∞) and zero ($u = 0$) at the cell surface (i.e. a no-slip condition). Using these two boundary conditions together with the Brinkman equation, fluid shear stress (τ) at the cell surface can be obtained as described in Supplementary Table S1B.

Statistical analysis

Data are presented as means ± S.D. Statistical comparison between two groups was performed by Student's t test. Multiple group comparison was performed by ANOVA with post hoc Bonferroni procedure unless noted otherwise. $P<0.05$ was considered statistically significant.

Results

Mouse hindlimb immobilization by spiral wiring induces atrophy and inflammatory responses of calf muscles

We first examined whether mouse hindlimb immobilization by spiral wiring, an animal model of disuse muscle atrophy that we previously developed [23], induced local inflammatory responses. Consistent with our previous observations, both the muscle mass of triceps surae and the CSA of gastrocnemius myofibers were significantly decreased by hindlimb immobilization (Figure 1B–D). Given no apparent damage or injury observed in muscle tissues of immobilized hindlimbs (Supplementary Figure S2C), these results indicate that calf muscles were atrophied by immobilization. Immunofluorescence staining revealed that cells expressing monocyte chemoattractant protein-1 (MCP-1) and tumor necrosis factor-α (TNF-α), both of which play key roles in regulating inflammatory processes [34,35], significantly increased in gastrocnemius muscle tissues of immobilized hindlimbs (MCP-1; Figure 1E,H,J, TNF-α; Figure 1F,I,K). Together with the increase in cells positively stained with F4/80, a marker for macrophages (Figure 1E,G,J,K), hindlimb immobilization appeared to instigate calf muscle atrophy involving local inflammatory responses including macrophage accumulation.

LCC attenuates immobilization-induced muscle atrophy with a modulation of inflammatory responses

We next examined whether massage-like mechanical interventions could modulate the pro-inflammatory effect of hindlimb immobilization on calf muscles. When we applied LCC (1 Hz, 30 min/day, see Supplementary Figure S1A) on mouse calves during the period of hindlimb immobilization, the CSA of gastrocnemius myofibers became significantly larger as compared with that in their contralateral control hindlimbs left unexposed to LCC (Figure 2C,D). Furthermore, LCC partially tempered the immobilization-induced decrease in contracting forces of triceps surae muscles (Figure 2E). In contrast, the muscle mass of triceps surae was not significantly different between immobilized hindlimbs with and without LCC application (Figure 2F). Because we observed a decrease in the interstitial space in LCC-applied gastrocnemius (Supplementary Figure S2D–F), we speculate that LCC tempered immobilization-induced edematous reactions of muscle tissues [36]. This in turn may have obscured the positive effects of LCC on muscle mass measured as a total wet tissue weight. In addition, LCC decreased the numbers of F4/80-positive, TNF-α-positive, and F4/80- MCP-1- or TNF-α- double positive cells in gastrocnemius muscle tissues of immobilized hindlimbs (F4/80; Figure 2G–I and Supplementary Figure S2G,H, MCP-1; Figure 2G,J and Supplementary Figure S2G, TNF-α; Figure 2H,K and Supplementary Figure S2H). Collectively, LCC alleviated local inflammatory responses including macrophage accumulation and immobilization-induced muscle atrophy. Notably, MCP-1 expression in intramuscular macrophages appeared to be enhanced by immobilization whereas this effect was tempered by LCC (Figure 2L and Supplementary Figure S2I). In contrast, TNF-α expression in macrophages was not significantly altered by immobilization or LCC (Figure 2M and Supplementary Figure S2J).

Clinical Science (2018) **132** 2147–2161
https://doi.org/10.1042/CS20180432

Depletion of macrophage recruited from circulating blood eliminates immobilization-induced muscle atrophy and inflammatory responses

The expression of MCP-1, which plays a crucial role in recruiting monocytes/macrophages from circulating blood [34], significantly increased prior to the decrease in both muscle mass and myofiber CSA upon immobilization (Figure 1C,D,H). Furthermore, MCP-1 expression increased more rapidly than that of TNF-α during the period of hindlimb immobilization (compare Figure 1H,I). Taken together, these results suggest that macrophage accumulation precedes muscle atrophy upon immobilization. We then asked whether this macrophage accumulation was due to the recruitment from circulating blood or proliferation/differentiation of local macrophages and their precursors, or both. To test this, we conducted hindlimb immobilization experiments using mice administered with clodronate liposomes (Supplementary Figure S1B). Clodronate liposomes induce apoptosis of phagocytic cells but cannot cross the capillary wall, thereby depleting circulating monocytes (Supplementary Figure S2K) and newly recruited macrophages but not muscle-resident macrophages or their precursors [37]. In clodronate liposome-administered mice, we did not observe significant decrease in the muscle mass of triceps surae and the CSA of gastrocnemius myofibers after hindlimb immobilization (Figure 3A–C, compare columns 2 and 5 in Figure 3B,C). Furthermore, hindlimb immobilization did not significantly increase the interstitial space in gastrocnemius muscles of those mice (compare columns 2 and 5 in Supplementary Figure S2L). Notably, the effects of daily LCC on the CSA of gastrocnemius myofibers (Figure 3C), the numbers of F4/80-, MCP-1-, and TNF-α-positive cells *in situ* (Figure 3D–J), and the gastrocnemius interstitial space (Supplementary Figure S2L) in immobilized hindlimbs were eliminated by clodronate liposome administration (compare columns 5 and 6 in each graph).

The number of F4/80-positive cells did not decrease in gastrocnemius muscles of mice injected with clodronate liposomes three times over 8 days (compare columns 1 and 2 in Figure 3F). This might be due to proliferation of macrophages derived from local precursors during prolonged clodronate liposome treatment [38]. In line with this, the number of F4/80-positive cells in gastrocnemius muscles was moderately increased by hindlimb immobilization even in clodronate liposome-administered mice (Figure 3D,E, compare columns 2 and 5 in Figure 3F). These results suggest that macrophages recruited from circulating blood, but not those derived from local precursors, play an important role in immobilization-induced muscle atrophy.

Analysis of interstitial fluid dynamics and simulative calculation of LCC-induced fluid shear stress on cells distributed in the interstitium of gastrocnemius muscle tissues

In muscle tissues, macrophages are distributed in their interstitial space. In addition to the intramuscular pressure waves (Figure 2B), our LCC procedure was most likely to generate interstitial fluid flow, leading to shear stress exertion on interstitial cells including macrophages. To estimate the effect of LCC on the interstitial fluid dynamics, we conducted μCT imaging using an iodine-based contrast medium (Isovist) injected to gastrocnemius muscle bellies (Supplementary Figure S1C). We found that LCC prompted interstitial fluid movement with a velocity of ∼50 μm/s (Figure 4A and Supplementary Figure S4B,C), indicating that intramuscular macrophages were subjected to FSS derived from interstitial flow during LCC. Using parameters including the amplitude of intramuscular pressure waves that we applied (Figure 2B) and the interstitial fluid viscosity reported previously [39,40] (Supplementary Table S1A), our simulative calculation suggests that intramuscular macrophages or other interstitial cells might be exposed to fluid shear stress with an average magnitude of 0.94–1.18 Pa during LCC (Supplementary Table S1B).

Fluid shear stress (FSS), but not hydrostatic pressure (HP), on macrophage *in vitro* reproduces the LCC effect on MCP-1 expression *in vivo*

To examine whether the responses of macrophage to LCC *in vivo* were mechanically relevant, we exposed cultured macrophages to pulsatile FSS or HP. We used thioglycolate-elicited peritoneal macrophages, which are enriched with monocyte-derived cells [41], because LCC appeared to modulate the function of macrophages recruited from circulating blood (Figure 3). Considering LCC tempered the immobilization-induced increase in MCP-1 expression in macrophages *in situ* (Figure 2L), we tested the response of macrophages treated with lipopolysaccharide (LPS), which promotes M1 polarization with enhanced MCP-1 expression [42]. We could stably apply pulsatile (frequency; 0.5 Hz) FSS with an average magnitude of 0.5 Pa or HP with amplitude of 50 mmHg on cultured macrophages for 30 min without apparent cell detachment (Supplementary Figure S3C). In the case of FSS experiments, the flow system was

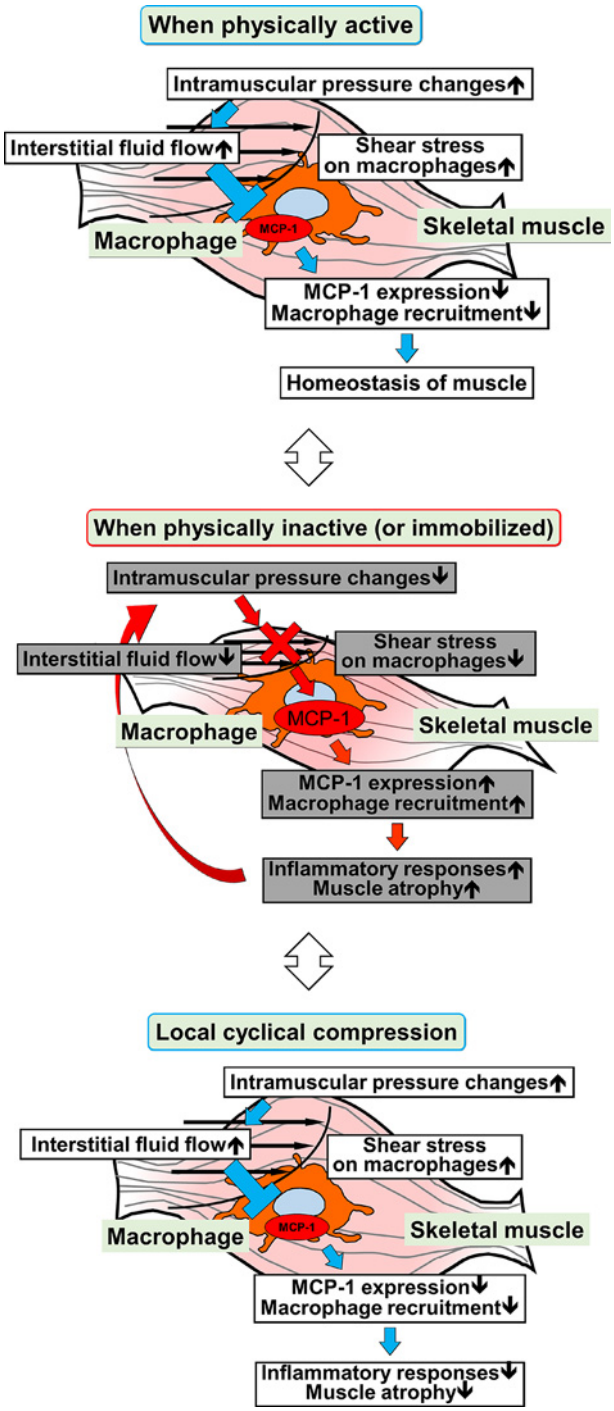

Figure 5. Schematic representation of the molecular mechanism behind the physical inactivity-induced atrophy of muscle as well as its restoration by LCC, involving the mechanosensory function of macrophages *in situ*

When physically active, muscle contraction generates intramuscular pressure changes, leading to interstitial fluid flow-induced shear stress exertion on macrophages *in situ* and suppression of inflammatory responses (top panel). When physically inactive, decrease or loss of intramuscular pressure changes leads to enhanced MCP-1 expression in macrophages, which results in muscle atrophy (middle panel). LCC restores intramuscular pressure changes, thereby hampering inflammatory responses and reversing muscle atrophy (bottom panel).

Clinical Science (2018) **132** 2147–2161
https://doi.org/10.1042/CS20180432

adjusted to generate 50 mmHg pressure waves to dissect shear stress-specific effects. On the other hand, the culture medium movement was kept minimal for HP experiments.

Thirty-minute FSS significantly decreased the expression of MCP-1, but not TNF-α, in LPS-treated peritoneal macrophages (Figure 4B), whereas application of HP alone for 30 min significantly enhanced both MCP-1 and TNF-α expressions (Supplementary Figure S3D). Notably, the expressions of other inflammation-related proteins, CD206 (anti-inflammatory) [43] and TGF-β1 (either pro- or anti-inflammatory) [44], were not significantly altered by FSS application. This suggests that the suppressive effect of FSS is fairly specific for MCP-1. In contrast, the increases in MCP-1 and TNF-α expressions and the decrease in CD206 expression after HP application (Supplementary Figure S3D) indicate that HP has pro-inflammatory properties.

We were unable to reliably apply pulsatile FSS with an average magnitude of ≥1 Pa or HP with a frequency of ≥1 Hz because of technical limitations concerning cell adhesion and precision of pressure control. We cannot thoroughly exclude the possibility that macrophages respond differently to FSS with higher magnitudes. However, anti-inflammatory effects have been reported to be more distinct in FSS with higher magnitudes on endothelial cells [45]. Therefore, intramuscular macrophages *in vivo*, which are expected to be exposed to FSS with ∼1 Pa during LCC (Supplementary Table S1), may respond more distinctly than we observed *in vitro* in terms of FSS-induced decrease in MCP-1 expression. All in all, our *in vivo* and *in vitro* data suggest that interstitial fluid flow caused by LCC is at least partially responsible for the LCC-induced decrease in MCP-1 expression in intramuscular macrophages (Figure 2L).

Discussion

Despite accumulating evidence regarding beneficial effects of physical exercise on health, it remains unclear how it modulates bodily functions. In this report, we have exemplified immobilization-induced muscle atrophy as a physical inactivity-induced disruption of organismal homeostasis. Our findings have clarified the significance of local mechanical stress or force on cells *in situ*, which appears to be at least partly responsible for positive effects of physical exercise.

The functions of macrophages have been extensively studied and their importance in the regulation of inflammatory processes has been firmly established. However, their mechano-sensing role is very poorly understood or hardly recognized. In the present study, we demonstrate that cultured macrophages are sensitive to FSS with an average magnitude of 0.5 Pa (Figure 4B). Together with the resistance of gastrocnemius muscle of clodronate liposome-administered mice to hindlimb immobilization (Figure 3A–C), mechanosensory function of macrophages recruited from circulating blood appears to be involved in tissue homeostasis. Whereas the decrease in MCP-1 expression in cultured macrophages by FSS relates to anti-inflammation, both pro- and anti-inflammatory effects of cyclical stretching of cultured macrophages have been reported [46,47]. Such variation might be due to the complexity of cyclical stretching, which is a combination of stretching and relaxation that can affect cellular signaling in opposite directions [48].

Interstitial fluid, which is the most abundant extracellular fluid with four-times volume as compared with circulating blood [49], is distributed throughout the entire body. Although the importance of interstitium in the regulation of organismal functions is being uncovered [50], interstitial fluid has been recognized to be mainly involved in local delivery of nutrients and removal of metabolic wastes [51]. To date, mechanical roles of interstitial fluid have not been demonstrated with very few exceptions including that in bone canaliculi that regulates bone homeostasis through FSS on osteocytes [52]. In the present study, we show that LCC, which generates intramuscular pressure waves mimicking the condition of mild muscle contraction [53], produces interstitial fluid flow, leading to shear stress exertion on macrophages *in situ*. Still, the majority of cells in parenchymal tissues are exposed to interstitial fluid, and mechano-sensing is a universal cellular function [54]. Therefore, it is possible that cells other than macrophages, such as satellite cells, also contribute to LCC-mediated alleviation of immobilization-induced muscle atrophy. The critical role of interstitial fluid flow as a cause of shear stress on cells *in situ* is compatible with the fact that edema, a condition characterized by local fluid accumulation and likely reduced interstitial fluid flow, is a representative symptom of local inflammation.

Bodily motions, with no exception, produce changes of stress distribution, i.e. local pressure changes, which generate interstitial fluid flow. Animals are defined so because of their ability to generate bodily motions voluntarily. Currently, the anti-inflammatory effects of FSS have been mainly shown for vascular endothelial cells with particular reference to its regularity and magnitude [55]. Our quantitative analysis of the interstitial fluid dynamics combined with our simulative calculation indicates that intramuscular interstitial cells are subjected to FSS with average magnitude of ∼1 Pa, which coincides with that exerted on vascular endothelial cells [56] or osteocytes [57]. Therefore, we

speculate that FSS of this range of magnitudes produced by bodily motions may be universally involved in organismal homeostasis.

Meanwhile, massage is defined as 'a mechanical manipulation of body tissues with rhythmical pressure and stroking for the purpose of promoting health and well-being' [58]. It perhaps unanimously agreed that massage relieves local pain/discomfort or even general unpleasantness/revolt. According to the American Massage Therapy Association, massage alleviates local soreness, headache, depression, and sleep disturbance, thereby improving quality of life (http://www.AMTA./org). However, there is a conflict concerning scientific evidence related to massage effects [59]. The anti-inflammatory effects of massage on skeletal muscles [14] have not been demonstrated with mechanistic insights, including those into the effector cells for massage. We have demonstrated LCC, a massage-like intervention, evokes interstitial flow, possibly leading to shear stress exertion on macrophages *in situ*. Our findings suggest the common mechanism behind the disuse muscle atrophy as well as the beneficial effects of physical exercise and massage (Figure 5). The present study may provide a cue to deciphering the essence of massage as a pain- and inflammation-relieving procedure and harnessing its effects toward a development of novel therapy.

Clinical perspectives

- While the importance and effectiveness of physical activity and exercise in human health is proven by several large-scale studies, the cellular and molecular mechanisms behind their beneficial effects are largely unknown.
- Massage-like mechanical interventions, which generate intramuscular pressure waves of amplitude equivalent to those during moderate muscle contraction, modulate macrophage recruitment, thereby alleviating inflammatory responses and immobilization-induced muscle atrophy.
- Our findings scientifically support the beneficial effects of massage, which have been recognized empirically.

Acknowledgments
We thank K. Nakanishi, K. Hamamoto, N. Kume, and K. Tsurumi for their consistent support throughout the project.

Author Contribution
Y.S. conceived the project, and Ku. S. conducted most of the experiments. M.T. and D.Y. conducted *in vitro* mechanical stress experiments (fluid shear stress and hydrostatic pressure application). N.S. conducted μCT analysis with support from M.M. D.Y. conducted simulative calculation of shear stress. A.T. and T.M. constructed the LCC apparatus. T.M. and N.S. conducted muscle contracting force measurements using the system that K.N. and K.K. developed. Y.R., M.N., N.K., Ka. S., T.O., I.H., S.K., Y.I., H.N., and T.S. provided technical and conceptual support and advice. Ku. S., M.T., Ke. S. and Y.S. wrote the manuscript.

Funding
This work was in part supported by Intramural Research Fund from the Japanese Ministry of Health, Labour and Welfare; Grants-in-Aid for Scientific Research from the Japan Society for the Promotion of Science (to T.O. and Y.S.); MEXT-Supported Program for the Strategic Research Foundation at Private Universities, 2015–2019 from the Japanese Ministry of Education, Culture, Sports, Science and Technology [S1511017]; and EMBO Long-Term Fellowship [ALTF 1130-2017 (to S.K.).

Competing Interests
The authors declare that there are no competing interests associated with the manuscript.

Abbreviations
CDN, clodronate; CSA, cross-sectional area; PBS, phosphate-buffered saline; LCC, local cyclical compression; LPS, lipopolysaccharide; MCP-1, monocyte chemoattractant protein-1; TNF-α, tumor necrosis factor-α; FSS, fluid shear stress; HP, hydrostatic pressure.

References
1 Lee, I.M., Shiroma, E.J., Lobelo, F., Puska, P., Blair, S.N. and Katzmarzyk, P.T. (2012) Effect of physical inactivity on major non-communicable diseases worldwide: an analysis of burden of disease and life expectancy. *Lancet* **380**, 219–229, https://doi.org/10.1016/S0140-6736(12)61031-9

2 Berg, H.E., Larsson, L. and Tesch, P.A. (1997) Lower limb skeletal muscle function after 6 wk of bed rest. *J. Appl. Physiol.* **82**, 182–188, https://doi.org/10.1152/jappl.1997.82.1.182
3 Caron, A.Z., Drouin, G., Desrosiers, J., Trensz, F. and Grenier, G. (2009) A novel hindlimb immobilization procedure for studying skeletal muscle atrophy and recovery in mouse. *J. Appl. Physiol.* **106**, 2049–2059, https://doi.org/10.1152/japplphysiol.91505.2008
4 Hunter, R.B., Stevenson, E., Koncarevic, A., Mitchell-Felton, H., Essig, D.A. and Kandarian, S.C. (2002) Activation of an alternative NF-κB pathway in skeletal muscle during disuse atrophy. *FASEB J.* **16**, 529–538, https://doi.org/10.1096/fj.01-0866com
5 Winkelman, C. (2004) Inactivity and inflammation: selected cytokines as biologic mediators in muscle dysfunction during critical illness. *AACN Clin. Issues* **15**, 74–82, https://doi.org/10.1097/00044067-200401000-00006
6 Al-Nassan, S., Fujita, N., Kondo, H., Murakami, S. and Fujino, H. (2012) Chronic exercise training down-regulates TNF-α and Atrogin-1/MAFbx in mouse gastrocnemius muscle atrophy induced by hindlimb unloading. *Acta Histochem. Cytochem.* **45**, 343–349, https://doi.org/10.1267/ahc.12023
7 Lira, F.S., Koyama, C.H., Yamashita, A.S., Rosa, J.C., Zanchi, N.E., Batista, Jr, M.L. et al. (2009) Chronic exercise decreases cytokine production in healthy rat skeletal muscle. *Cell. Biochem. Funct.* **27**, 458–461, https://doi.org/10.1002/cbf.1594
8 Dogra, S., Ashe, M.C., Biddle, S.J.H., Brown, W.J., Buman, M.P., Chastin, S. et al. (2017) Sedentary time in older men and women: an international consensus statement and research priorities. *Br. J. Sports Med.* **51**, 1526–1532, https://doi.org/10.1136/bjsports-2016-097209
9 Hamilton, M.T., Healy, G.N., Dunstan, D.W., Zderic, T.W. and Owen, N. (2008) Too little exercise and too much sitting: inactivity physiology and the need for new recommendations on sedentary behavior. *Curr. Cardiovasc. Risk Rep.* **2**, 292–298, https://doi.org/10.1007/s12170-008-0054-8
10 Furlan, A.D., Giraldo, M., Baskwill, A., Irvin, E. and Imamura, M. (2015) Massage for low back pain: an updated systematic review within the framework of the Cochrane Back Review Group. *Spine* **34**, 1669–1684, https://doi.org/10.1097/BRS.0b013e3181ad7bd6
11 Robertson, A., Watt, J. and Galloway, S. (2004) Effects of leg massage on recovery from high intensity cycling exercise. *Br. J. Sports Med.* **38**, 173–176, https://doi.org/10.1136/bjsm.2002.003186
12 Waters-Banker, C., Butterfield, T.A. and Dupont-Versteegden, E.E. (2014) Immunomodulatory effects of massage on nonperturbed skeletal muscle in rats. *J. Appl. Physiol.* **116**, 164–175, https://doi.org/10.1152/japplphysiol.00573.2013
13 Haas, C., Butterfield, T.A., Abshire, S., Zhao, Y., Zhang, X., Jarjoura, D. et al. (2013) Massage timing affects postexercise muscle recovery and inflammation in a rabbit model. *Med. Sci. Sports Exerc.* **45**, 1105–1112, https://doi.org/10.1249/MSS.0b013e31827fdf18
14 Crane, J.D., Ogborn, D.I., Cupido, C., Melov, S., Hubbard, A., Bourgeois, J.M. et al. (2012) Massage therapy attenuates inflammatory signaling after exercise-induced muscle damage. *Sci. Transl. Med.* **4**, 119ra113, https://doi.org/10.1126/scitranslmed.3002882
15 Stewart, L.K., Flynn, M.G., Campbell, W.W., Craig, B.A., Robinson, J.P., Timmerman, K.L. et al. (2007) The influence of exercise training on inflammatory cytokines and C-reactive protein. *Med. Sci. Sports Exerc.* **39**, 1714–1719, https://doi.org/10.1249/mss.0b013e31811ece1c
16 Timmerman, K.L., Flynn, M.G., Coen, P.M., Markofski, M.M. and Pence, B.D. (2008) Exercise training-induced lowering of inflammatory (CD14+CD16+) monocytes: a role in the anti-inflammatory influence of exercise? *J. Leukoc. Biol.* **84**, 1271–1278, https://doi.org/10.1189/jlb.0408244
17 Acharyya, S., Villalta, S.A., Bakkar, N., Bupha-Intr, T., Janssen, P.M., Carathers, M. et al. (2007) Interplay of IKK/NF-κB signaling in macrophages and myofibers promotes muscle degeneration in Duchenne muscular dystrophy. *J. Clin. Invest.* **117**, 889–901, https://doi.org/10.1172/JCI30556
18 Kang, X., Hou, A., Wang, R., Liu, D., Xiang, W., Xie, Q. et al. (2016) Macrophage TCF-4 co-activates p65 to potentiate chronic inflammation and insulin resistance in mice. *Clin. Sci.* **130**, 1257–1268, https://doi.org/10.1042/CS20160192
19 Kirstein, M., Brett, J., Radoff, S., Ogawa, S., Stern, D. and Vlassara, H. (1990) Advanced protein glycosylation induces transendothelial human monocyte chemotaxis and secretion of platelet-derived growth factor: role in vascular disease of diabetes and aging. *Proc. Natl. Acad. Sci. U.S.A.* **87**, 9010–9014, https://doi.org/10.1073/pnas.87.22.9010
20 Yasojima, K., Schwab, C., McGeer, E.G. and McGeer, P.L. (2001) Complement components, but not complement inhibitors, are upregulated in atherosclerotic plaques. *Arterioscler. Thromb. Vasc. Biol.* **21**, 1214–1219, https://doi.org/10.1161/hq0701.092160
21 McGeer, P.L. and McGeer, E.G. (2004) Inflammation and the degenerative diseases of aging. *Ann. NY Acad. Sci.* **1035**, 104–116, https://doi.org/10.1196/annals.1332.007
22 Simpson, E.R. and Brown, K.A. (2013) Minireview: Obesity and breast cancer: a tale of inflammation and dysregulated metabolism. *Mol. Endocrinol.* **27**, 715–725, https://doi.org/10.1210/me.2013-1011
23 Onda, A., Kono, H., Jiao, Q., Akimoto, T., Miyamoto, T., Sawada, Y. et al. (2016) New mouse model of skeletal muscle atrophy using spiral wire immobilization. *Muscle Nerve* **54**, 788–791, https://doi.org/10.1002/mus.25202
24 Mori, Y., Chen, T., Fujisawa, T., Kobashi, S., Ohno, K., Yoshida, S. et al. (2014) From cartoon to real time MRI: in vivo monitoring of phagocyte migration in mouse brain. *Sci. Rep.* **4**, 6997, https://doi.org/10.1038/srep06997
25 Ma, Y., Li, Y., Jiang, L., Wang, L., Jiang, Z., Wang, Y. et al. (2016) Macrophage depletion reduced brain injury following middle cerebral artery occlusion in mice. *J. Neuroinflammation.* **13**, 38, https://doi.org/10.1186/s12974-016-0504-z
26 Strober, W. (2000) Wright-Giemsa and nonspecific esterase staining of cells. *Curr. Protoc. Cytom.* **11**, A.3D.1–A.3D.4
27 Lee, S.H., Starkey, P.M. and Gordon, S. (1985) Quantitative analysis of total macrophage content in adult mouse tissues. Immunochemical studies with monoclonal antibody F4/80. *J. Exp. Med.* **161**, 475–489, https://doi.org/10.1084/jem.161.3.475
28 Fortier, A.H. and Falk, L.A. (1994) Isolation of murine macrophages. *Curr. Protoc. Immunol.* **11**, 14.11.11–14.11.19
29 Jenkins, S.J., Ruckerl, D., Cook, P.C., Jones, L.H., Finkelman, F.D., van Rooijen, N. et al. (2011) Local macrophage proliferation, rather than recruitment from the blood, is a signature of Th2 inflammation. *Science* **332**, 1284–1288, https://doi.org/10.1126/science.1204351
30 Stuart, W.D., Kulkarni, R.M., Gray, J.K., Vasiliauskas, J., Leonis, M.A. and Waltz, S.E. (2011) Ron receptor regulates Kupffer cell-dependent cytokine production and hepatocyte survival following endotoxin exposure in mice. *Hepatology* **53**, 1618–1628, https://doi.org/10.1002/hep.24239
31 Yoshino, D., Sakamoto, N., Takahashi, K., Inoue, E. and Sato, M. (2013) Development of novel flow chamber to study endothelial cell morphology: effects of shear flow with uniform spatial gradient on distribution of focal adhesion. *JBSE* **8**, 233–243, https://doi.org/10.1299/jbse.8.233

32 Yoshino, D., Sato, K. and Sato, M. (2015) Endothelial cell response under hydrostatic pressure condition mimicking pressure therapy. *Cell. Mol. Bioeng.* **8**, 296–303, https://doi.org/10.1007/s12195-015-0385-8
33 Ogasawara, R., Kobayashi, K., Tsutaki, A., Lee, K., Abe, T., Fujita, S. et al. (2013) mTOR signaling response to resistance exercise is altered by chronic resistance training and detraining in skeletal muscle. *J. Appl. Physiol.* **114**, 934–940, https://doi.org/10.1152/japplphysiol.01161.2012
34 Luster, A.D. (1998) Chemokines - chemotactic cytokines that mediate inflammation. *N. Engl. J. Med.* **338**, 436–445, https://doi.org/10.1056/NEJM199802123380706
35 Reid, M.B. and Li, Y.-P. (2001) Tumor necrosis factor-α and muscle wasting: a cellular perspective. *Respir. Res.* **2**, 269, https://doi.org/10.1186/rr67
36 Reed, R.K. (1981) Interstitial fluid volume, colloid osmotic and hydrostatic pressures in rat skeletal muscle. Effect of venous stasis and muscle activity.. *Acta Physiol. Scand.* **112**, 7–17
37 Van Rooijen, N. (1989) The liposome-mediated macrophage 'suicide' technique. *J. Immunol Methods* **124**, 1–6, https://doi.org/10.1016/0022-1759(89)90178-6
38 Côté, C.H., Bouchard, P., van Rooijen, N., Marsolais, D. and Duchesne, E. (2013) Monocyte depletion increases local proliferation of macrophage subsets after skeletal muscle injury. *BMC Musculoskelet. Disord.* **14**, 359, https://doi.org/10.1186/1471-2474-14-359
39 Zurovsky, Y., Mitchell, G. and Hattingh, J. (1995) Composition and viscosity of interstitial fluid of rabbits. *Exp. Physiol.* **80**, 203–207, https://doi.org/10.1113/expphysiol.1995.sp003840
40 Shorten, P.R., McMahon, C.D. and Soboleva, T.K. (2007) Insulin transport within skeletal muscle transverse tubule networks. *Biophys. J.* **93**, 3001–3007, https://doi.org/10.1529/biophysj.107.107888
41 Ghosn, E.E., Cassado, A.A., Govoni, G.R., Fukuhara, T., Yang, Y., Monack, D.M. et al. (2010) Two physically, functionally, and developmentally distinct peritoneal macrophage subsets. *Proc. Natl. Acad. Sci. U.S.A.* **107**, 2568–2573, https://doi.org/10.1073/pnas.0915000107
42 Lu, H.L., Huang, X.Y., Luo, Y.F., Tan, W.P., Chen, P.F. and Guo, Y.B. (2018) Activation of M1 macrophages plays a critical role in the initiation of acute lung injury. *Biosci. Rep.* **38**, BSR20171555, https://doi.org/10.1042/BSR20171555
43 Porcheray, F., Viaud, S., Rimaniol, A.C., Léone, C., Samah, B., Dereuddre-Bosquet, N. et al. (2005) Macrophage activation switching: an asset for the resolution of inflammation. *Clin. Exp. Immunol.* **142**, 481–489
44 Sanjabi, S., Zenewic, zL.A., Kamanaka, M. and Flavell, R.A. (2009) *Curr. Opin. Pharmacol.* **9**, 447–453, https://doi.org/10.1016/j.coph.2009.04.008
45 Malek, A.M., Alper, S.L. and Izumo, S. (1999) Hemodynamic shear stress and its role in atherosclerosis. *JAMA* **282**, 2035–2042, https://doi.org/10.1001/jama.282.21.2035
46 Wehner, S., Buchholz, B.M., Schuchtrup, S., Rocke, A., Schaefer, N., Lysson, M. et al. (2010) Mechanical strain and TLR4 synergistically induce cell-specific inflammatory gene expression in intestinal smooth muscle cells and peritoneal macrophages. *Am. J. Physiol. Gastrointest. Liver Physiol.* **299**, G1187–1197, https://doi.org/10.1152/ajpgi.00452.2009
47 Maruyama, K., Sakisaka, Y., Suto, M., Tada, H., Nakamura, T., Yamada, S. et al. (2018) Cyclic stretch negatively regulates IL-1β secretion through the inhibition of NLRP3 inflammasome activation by attenuating the AMP kinase pathway. *Front. Physiol.* **9**, 802, https://doi.org/10.3389/fphys.2018.00802
48 Sawada, Y., Nakamura, K., Doi, K., Takeda, K., Tobiume, K., Saitoh, M. et al. (2001) Rap1 is involved in cell stretching modulation of p38 but not ERK or JNK MAP kinase. *J. Cell Sci.* **114**, 1221–1227
49 Davies, B. and Morris, T. (1993) Physiological parameters in laboratory animals and humans. *Pharm. Res.* **10**, 1093–1095, https://doi.org/10.1023/A:1018943613122
50 Benias, P.C., Wells, R.G., Sackey-Aboagye, B., Klavan, H., Reidy, J., Buonocore, D. et al. (2018) Structure and distribution of an unrecognized Interstitium in human tissues. *Sci. Rep.* **8**, 4947, https://doi.org/10.1038/s41598-018-23062-6
51 Jéquier, E. and Constant, F. (2009) Water as an essential nutrient: the physiological basis of hydration. *Eur. J. Clin. Nutr.* **64**, 115, https://doi.org/10.1038/ejcn.2009.111
52 Bonewald, L.F. (2006) Mechanosensation and transduction in osteocytes. *Bone* **3**, 7–15
53 McDermott, A.G.P., Marble, A.E., Yabsley, R.H. and Phillips, M.B. (1982) Monitoring dynamic anterior compartment pressures during exercise:A new technique using the STIC catheter. *Am. J. Sports Med.* **10**, 83–89, https://doi.org/10.1177/036354658201000204
54 Discher, D., Dong, C., Fredberg, J.J., Guilak, F., Ingber, D., Janmey, P. et al. (2009) Biomechanics: cell research and applications for the next decade. *Ann. Biomed. Eng.* **37**, 847–859, https://doi.org/10.1007/s10439-009-9661-x
55 Yamawaki, H., Pan, S., Lee, R.T. and Berk, B.C. (2005) Fluid shear stress inhibits vascular inflammation by decreasing thioredoxin-interacting protein in endothelial cells. *J. Clin. Invest.* **115**, 733–738, https://doi.org/10.1172/JCI200523001
56 Kovacs, G., Berghold, A., Scheidl, S. and Olschewski, H. (2009) Pulmonary arterial pressure during rest and exercise in healthy subjects: a systematic review. *Eur. Respir. J.* **34**, 888–894, https://doi.org/10.1183/09031936.00145608
57 Kwon, R.Y., Meays, D.R., Tang, W.J. and Frangos, J.A. (2010) Microfluidic enhancement of intramedullary pressure increases interstitial fluid flow and inhibits bone loss in hindlimb suspended mice. *J. Bone Miner. Res.* **25**, 1798–1807, https://doi.org/10.1002/jbmr.74
58 Cafarelli, E. and Flint, F. (1992) The role of massage in preparation for and recovery from exercise. *Sports Med.* **14**, 1–9, https://doi.org/10.2165/00007256-199214010-00001
59 Best, T.M., Hunter, R., Wilcox, A. and Haq, F. (2008) Effectiveness of sports massage for recovery of skeletal muscle from strenuous exercise. *Clin. J. Sport Med.* **18**, 446–460, https://doi.org/10.1097/JSM.0b013e31818837a1